Applied Clay Science 287 (2026) 108191

Contents lists available at ScienceDirect

Applied Clay Science

journal homepage: www.elsevier.com/locate/clay

Research Paper

A permselective membrane for size-sieving based H_2/CO_2 separation

Lukas Federer, Ingmar Pietsch, Felix Uhlig, Max Stevenson, Daniel Friedrich [1], Josef Breu [*,2]

Department of Chemistry, Chair of Inorganic Colloids for Electrochemical Energy storage, University of Bayreuth, 95440 Bayreuth, Germany

ARTICLE INFO

Keywords:
H_2 separation/purification
Permselective membrane
Clay
Nanosheets
2D layered materials
1D monodomain Bragg stacks

ABSTRACT

Continuous H_2/CO_2 separation via permselective membranes is highly sought after as pure H_2 plays a key role in H_2 economy. Aqueous nematic suspensions obtained by 1D dissolution of affordable sodium fluorohectorite allow for simple membrane fabrication by spray coating. The monolayer nanosheets have a uniform thickness of 1 nm and appreciable aspect ratio, thus self-assemble into defect-free membranes when applied onto porous mixed cellulose ester substrates. The perfectly textured restacking of individual nanosheets yields monodomain Bragg stacks with uniform interlayer space. By cation exchange with guanidinium cations, a uniform interlayer height tailored to 2.9 Å was obtained while micropores are formed between the loosely packed interlayer cations. As the interlayer height matches the kinetic diameter of H_2 and is significantly smaller compared to other relevant gas species, e. g. CO_2, CH_4, CO or N_2, perfectly selective H_2 sieving may be obtained. In a Wicke-Kallenbach cell, a near-perfect separation of H_2 and CO_2 (4:1 ratio) at ambient conditions was obtained. The tortuous path created by the impermeable, large aspect ratio nanosheets reduces the permeance to disappointing 3 GPU (gas permeation units; 1 GPU = 10^{-6} cm^3 cm^{-2} s^{-1} $cmHg^{-1}$). While the separation mechanism playing on tortuous path has not been fully explored in this preliminary study, the permeance may be improved substantially in future studies by optimizing the roughness of the substrate, the aspect ratio of the nanosheets and the thickness of the membrane.

1. Introduction

Hydrogen (H_2) is a key component of the green deal of the European Union (Yue et al., 2021; Miłek et al., 2022). In 2022, the total annual H_2 demand was considered to be some 90 million tons (Wappler et al., 2022), and the demand is rising. Ammonia synthesis, e. g. for fertilizers, and methanol production represent the largest sectors (Ritter and Ebner, 2007; Wappler et al., 2022). While electrolysis is the only production method that yields clean (green) H_2 (Hassan et al., 2024), the majority of H_2 originates from sources that need some kind of separation or cleaning. The largest proportion of the world's H_2 is produced from fossil fuels (Sun et al., 2024). This need for purification, however, not only applies to chemically produced H_2 but also to biomass derived H_2 (Holladay et al., 2009) and geological H_2 resources that recently attracted attention (Ellis and Gelman, 2024).

Fractional/cryogenic distillation and pressure swing adsorption are the main commercial processes applied to separate/purify H_2 (Sircar and Golden, 2000; Ockwig and Nenoff, 2007). However, these processes require considerable energy, rendering them cost-intensive (Chuah et al., 2020). The lack of purity of H_2 obtained by these processes is another issue that makes it difficult or even impossible to use the gas in certain H_2 economy applications, as a majority of applications require a H_2 purity of at least 99.99% (Ockwig and Nenoff, 2007; Al-Mufachi et al., 2015).

In a continuous process, separation of H_2 needs permselective membranes that are permeable for H_2 but impermeable for larger relevant gas molecules like carbon dioxide (CO_2), methane (CH_4), carbon monoxide (CO) and nitrogen (N_2). The main advantages of membrane-based technologies are the improved energy efficiency and the continuous operation, allowing for a simultaneous feed of the gas mixture and discharge of the purified gas (Spillman, 1989; Bredesen et al., 2004; Adhikari and Fernando, 2006; Ockwig and Nenoff, 2007; Peng et al., 2014; Sazali et al., 2020; Sun et al., 2024).

A broad variety of membranes have been established for H_2

* Corresponding author at: Department of Chemistry; Chair of Inorganic Colloids for Electrochemical Energy storage; University of Bayreuth, 95440 Bayreuth, Germany.
E-mail address: josef.breu@uni-bayreuth.de (J. Breu).
[1] 0000–0001–6953-8114
[2] 0000–0002–2547-3950

https://doi.org/10.1016/j.clay.2026.108191
Received 25 November 2025; Received in revised form 13 March 2026; Accepted 14 March 2026
Available online 24 March 2026

separation. These range from inorganic membranes such as metallic, ceramic (silica/zeolite) and carbon-based membranes over organic membranes such as polymer, metal organic framework and covalent organic framework membranes to mixed matrix membranes, as summarized in reviews (Ockwig and Nenoff, 2007; Li et al., 2015; Sun et al., 2024). While inorganic membranes show relatively low fluxes and typically complex manufacturing processes, the downside of organic membranes is ageing, which results in reduced separation performance over time (Wang et al., 2018; Sun et al., 2024). Targeted control of the structure also represents another major challenge with the organic membranes, while mixed matrix membranes exhibit compatibility difficulties with the inorganic fillers and organic polymer matrix (Sun et al., 2024). Membranes for gas separation operate on three different mechanisms: i) adsorption diffusion, ii) solution diffusion and iii) molecular sieving (Sun et al., 2024).

Molecular sieving with membranes can be achieved by the fabrication of a dense, defect-free, thin coat on a porous substrate (Heinke et al., 2015). The coat, however, must also be selectively permeable for H_2. Nanoporous two dimensional (2D) laminated membranes have proven attractive materials for molecular separation and related areas (Kim and Nair, 2013. The large aspect ratios of nanosheets allow for self-assembly of continuous large area one dimensional (1D) crystalline monodomains by lateral overlap of the 2D building blocks (Schuchardt et al., 2023). This is crucial as the nanosheets may be as thin as 1 nm and very thin (few μm or even thinner) membranes may be cast that minimize transport resistance. This is crucial as permeance and separation factor are usually inversely correlated in membrane-based gas separation (Liu et al., 2015). Molecular sieving may be achieved either through applying (ultra-)microporous nanosheets (Agrawal et al., 2011; Peng et al., 2014; Dakhchoune et al., 2021) or through the height of the interlayer space (Liu et al., 2014a). Precise control of the interlayer height requires strictly monolayer nanosheets that are spread open by molecular pillars of an appropriate size assuring H_2 selectivity. Size-exclusion must show high selectivity as the kinetic diameters of H_2 (2.89 Å (Mehio et al., 2014)) and for instance CO_2 (3.30 Å (Mehio et al., 2014)) differ little.

Melt-synthesized fluorohectorite of nominal composition $[Na_{0.5}]^{inter}[Mg_{2.5}Li_{0.5}]^{oct}[Si_4]^{tet}O_{10}F_2$ (NaHec) (Breu et al., 2001) may be delaminated by a thermodynamically driven process labeled 1D dissolution (Rosenfeldt et al., 2016; Dudko et al., 2023). The spontaneous nature yields strictly monolayer dispersions of 1 nm thin nanosheets with huge aspect ratios that hamper rotation. Thus, lamellar liquid crystalline, nematic suspensions are obtained where adjacent nanosheets are held in coplanar arrangement. When applying a wet coat, e.g. by spray coating of these suspensions on flat substrates, 1D crystalline, monodomain Bragg stack films are obtained (Schuchardt et al., 2023). The deposition of delaminated (clay) nanosheets into textured films by spray coating has been reported by several authors (Tsurko et al., 2017; Zhou et al., 2019; Abd-Elrahim and Chun, 2022; Nunnenkamp et al., 2022; Shi et al., 2023; Sudo et al., 2025).

In this work, this 1D crystalline, monodomain Bragg stack nature of a spray-coated hectorite film is exploited to fabricate perfectly textured membranes for gas separation applications. In this context, the exchangeability of the $[Na(H_2O)_6]^+$ interlayer cations in the pristine NaHec film with appropriate cations is the decisive factor in achieving a tailored, uniform interlayer height between individual silicate nanosheets that can be adapted to the desired gas separation by size exclusion depending on the interlayer height as defined by the molecular dimensions of the pillar species. This results in high flexibility and thus a wide range of applicability due to a large selection of available pillar molecules, enabling precise control of the interlayer height. Here, by exchanging the pristine $[Na(H_2O)_6]^+$ interlayer cations with less hydrophilic and thus non-hydrated guanidinium (Gua) cations, the interlayer height in the fabricated Gua intercalated hectorite (GuaHec) membrane was adjusted to 2.9 Å, which allows for molecular sieving of H_2 and thereby enabling separation of H_2 from CO_2, which is pivotal in the steam reforming of CH_4.

2. Experimental section

2.1. Materials

Sodium fluorohectorite of the nominal composition $[Na_{0.5}]^{inter}[Mg_{2.5}Li_{0.5}]^{oct}[Si_4]^{tet}O_{10}F_2$ (NaHec) (cation exchange capacity: 118 mEq/100 g) was obtained by melt synthesis in a closed molybdenum crucible according to a previously published procedure (Breu et al., 2001). Guanidine hydrochloride ($CH_5N_3 \cdot HCl$; CAS: 50–01-1; purity ≥99.5%) was purchased from Carl Roth GmbH + Co. KG and used without further purification. A mixed cellulose ester (MCE) membrane filter with a pore size of 0.8 μm was purchased from Pall (GN-4 Metricel; P/N 64678) and used as substrate without further treatment. H_2 (3.0), CO_2 (4.5), Ar (5.0) and He (5.0) were supplied by Rießner-Gase.

2.2. Preparation of NaHec suspensions

A 0.5 wt% NaHec suspension was obtained by 1D dissolution of the as-synthesized NaHec in double distilled water. The 0.5 wt% NaHec suspension with smaller platelet size was obtained by using a M110Y Microfluidizer from Microfluidics (1 cycle, 1.2 kbar).

2.3. Preparation of the NaHec film

The NaHec film was prepared by using a fully automatic spray coating system with an infrared lamp drying unit. The pressure used for spray coating was 2 bar. The film was dried for 90 s at a temperature of 40 °C after every spray cycle. First, 10 cycles of the as obtained 0.5 wt% NaHec suspension were spray coated on the MCE substrate. Second, 100 cycles of the 0.5 wt% NaHec suspension with smaller platelet size were spray coated on top.

2.4. Preparation of the GuaHec membrane

The GuaHec membrane was obtained by cation exchange at room temperature. For this purpose, 2 mL of a 1 M guanidine hydrochloride solution was dripped onto the surface of the prepared NaHec film using a pipette until the entire surface of the film was completely covered with the solution. After approx. 24 h, the exchange solution was replaced with a fresh one. To do this, the old solution was drained off by tilting the Petri dish containing the film and subsequently adding a fresh exchange solution on top of the surface in the same way as described above. To ensure complete cation exchange, the solution was replaced a total of five times, with an exposure time of 24 h each. After that, the membrane was thoroughly washed with water to remove excess of guanidine hydrochloride. The membrane was dried and stored under ambient conditions.

2.5. Preparation of bulk GuaHec for TGA and Ar physisorption

4 g NaHec powder were add to a solution of 567 mg guanidine hydrochloride (excess of 25%) in 20 mL double distilled water. After shaking overhead overnight at room temperature, the product was thoroughly washed with water to remove excess of guanidine hydrochloride, dried at 90 °C overnight and stored under ambient conditions. The XRD pattern (**Fig. S1**) and the EDX analysis (**Fig. S2**) of bulk GuaHec confirm complete cation exchange.

2.6. Static light scattering (SLS)

SLS analyses of highly diluted NaHec suspensions (as-synthesized and shredded, respectively) were carried out with a HORIBA LA-950 to record the particle size distributions. A measurement routine called “mica H2O” (supplied by the manufacturer) was applied using a refractive index of the solid phase of 1.59.

2.7. X-ray diffraction (XRD)

XRD patterns were recorded with an EMPYREAN diffractometer (PANalytical) in Bragg-Brentano geometry, which was operated with Cu-Kα radiation ($\lambda = 1.5418$ Å) and a PIXcel 1D-Medipix3 detector. For that, a small piece of the NaHec film and the GuaHec membrane, respectively, was detached from the substrate and placed on a microscope slide. The bulk GuaHec sample was prepared by casting a suspension of bulk GuaHec onto a microscope slide followed by subsequent drying. The XRD patterns were analyzed using the X'Pert HighScore Plus software from PANalytical (version 3.0). Reflections resulting from Cu-Kα_2 radiation were stripped with the software.

2.8. Scanning electron microscopy (SEM) and energy-dispersive X-ray (EDX) spectroscopy

For SEM and EDX analysis, the dry materials (powder of bulk GuaHec and a small piece of GuaHec membrane detached from substrate, respectively) were attached to a carbon tape and sputtered with 20 nm carbon. The analysis was carried out on a Zeiss Ultra plus: High-resolution field emission scanning electron microscope with 80 mm sample gate, inlens detector and UltraDry EDS detector (30 mm^2) (Thermo Fisher Scientific NS7).

2.9. Transmission electron microscopy (TEM)

For cross-sectional TEM images, the GuaHec membrane (small piece detached from substrate) was thinned with a JEOL IB-09060CIS Cryo Ion Slicer. TEM images were acquired using a JEOL JEM-2200FS Field Emission Energy Filter Transmission Electron Microscope (FEEFTEM) operated at an accelerating voltage of 200 kV. Lossless filtered microscope images ($\Delta E \sim 0$ eV) were acquired with a bottom-mounted CMOS camera system (OneView, Gatan) and processed with DM 3.3 image processing software (Gatan). The images were analyzed using ImageJ (version 1.53k).

2.10. Thermogravimetric analysis (TGA)

TGA of bulk GuaHec was carried out with a NETZSCH STA 449C with a heating rate of 10 K min^{-1} in air. The data was analyzed using NETZSCH Proteus Thermal Analysis software (version 6.1.0). The thermogravimetric analysis of the non-coated MCE substrate was carried out with a STA PT1600 from Linseis with a heating rate of 10 K min^{-1} in air.

2.11. Ar physisorption measurement

Prior to the measurement, the sample was degassed in a high vacuum at 120 °C for 24 h. Ar physisorption measurements were performed with a Quantachrome Autosorb 1 at Ar(l) temperature (87.35 K). The Autosorb 1 was equipped with a Quantachrome CryoSync cryostat. The data were analyzed using the Quantachrome ASiQwin software package (version 3.0).

2.12. Evaluation of separation performance

For evaluation of the separation performance a customized Wicke-Kallenbach cell was integrated in a mixSorb S Dynamic Sorption Analyzer from 3P Instruments. The GuaHec membrane was encapsulated on both sides in an adhesive aluminum mask (outer diameter of 32 mm; inner diameter of 10 mm) to prevent mechanical demolition when inserting the membrane airtight (use of silicon O-ring) into the cell. Before the measurement the membrane was flushed with He (10 mL min^{-1}; feed) and Ar (10 mL min^{-1}; sweep) for 1 h. The measurement was done at ambient conditions (23.4 °C and 1 bar) with 8 mL min^{-1} H_2 flow and 2 mL min^{-1} CO_2 flow on the feed gas side (total flow of 10 mL min^{-1}) and 10 mL min^{-1} Ar flow on the sweep gas side. During measurement, no pressure difference between feed gas side and permeate gas side was observed. The permeate was analyzed with an online mass-selective detector calibrated to the gas mixture to be measured with the empty cell prior to measurement. The mass spectrometer used was an Omnistar GSD 320 from Pfeiffer Vacuum. The measurement was carried out until a steady state was reached. The data was analyzed using the QUADERA software package from Pfeiffer Vacuum (version 4.62). The same procedure was done with pure MCE substrate. The equations for determination of permeance and separation factor from these measurements are shown in supporting information.

3. Results and discussion

3.1. Fabrication of the membrane

In water, spontaneous, thermodynamically driven delamination by 1D dissolution of NaHec is observed (Dudko et al., 2023), yielding individual monolayer nanosheets with 1 nm thickness and a large mean diameter of about 20 μm according to static light scattering (SLS) analysis (**Fig. S3**). Thus, pristine NaHec nanosheets are obtained showing large aspect ratios of 20,000 on average and a unique homogeneous layer charge distribution (Breu et al., 2001; Stöter et al., 2013). The resulting liquid crystalline, nematic phase allows for simple water-based processing. Spray coating of this suspension enables the fabrication of a crystalline monodomain NaHec film by perfectly textured self-assembly of the nanosheets which orient parallel to the planar substrate due to the high aspect ratio (Fig. 1). A MCE membrane filter was used as a model substrate. This substrate has pores of 0.8 μm diameter and consequently a noticeable surface roughness. As the pores of the substrate are orders of magnitude larger compared to the kinetic diameters of various gases, the substrate has not any impact on the gas separation by molecular sieving.

To bridge the pores and smoothen the surface, 10 wet coats (thickness of a few μm) of a 0.5 wt% nematic suspension of the as-synthesized NaHec were applied first, resulting in a dry coating thickness of about 140 nm (Schuchardt et al., 2023). The large aspect ratio, however, leads to the buildup of a long tortuous path as the nanosheets are made up by a dense, brucitic octahedral sheet, sandwiched between two tetrahedral sheets that are even impermeable for H_2 or He (Habel et al., 2020). The permeance is decreasing with the square of the aspect ratio (DeRocher et al., 2005). H_2 is capable to diffuse along the slit confined between two nanosheets parallel to the membrane. Cross diffusion is only possible in the larger gaps between two edge facing nanosheets. In a defect-free film made from a nematic suspension, adjacent nanosheets are stacked with shifts relative to each other. Gaps between edge facing individual nanosheets are statistically almost never arranged on top of each other and therefore any gases too large to diffuse along the slits will be completely blocked. While slit selectivity assures sieving of H_2, the permeance will be limited by the generated tortuous path. Therefore, the body of the membrane was manufactured by nanosheets of greatly reduced aspect ratio produced by microfluidizing the pristine NaHec suspension. 100 wet coats of a 0.5 wt% nematic suspension of diameter reduced NaHec platelets with a mean diameter of about 3 μm (**Fig. S3**) were spray-coated on top of the primer coat.

The NaHec film obtained by spray coating represents a monodomain Bragg stack film as evidenced by the X-ray diffraction (XRD) pattern showing a highly rational 00l-series with a d-value given by the 001-reflection of 15.3 Å at approx. 90% relative humidity (rH) (Fig. 2a) (Stöter et al., 2013). The calculated coefficient of variation of the NaHec film is <0.75%, indicating a perfectly periodic homogeneous arrangement of the platelets after self-assembled restacking. This Bragg stack nature of the membrane is unique to the utterly delaminated, monolayer nanosheets with a perfectly defined uniform interlayer height.

As mentioned above, monolayers are crucial for the fabrication of perfectly ordered membranes. Literature, however, also reports other

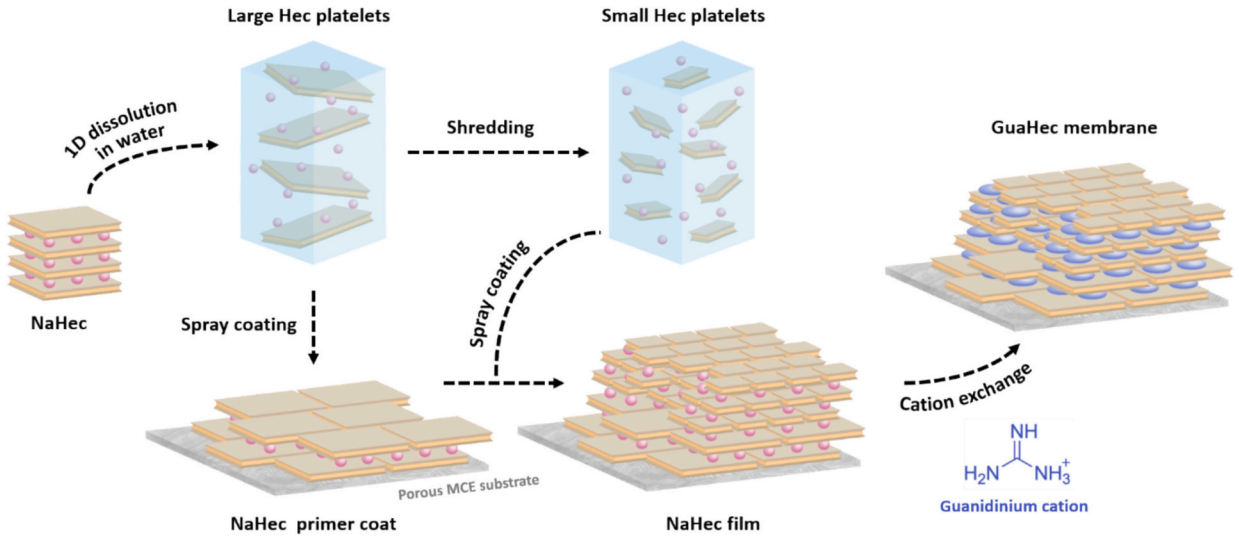

Fig. 1. Schematic illustration of the fabrication process of a guanidinium (Gua) intercalated hectorite (GuaHec) membrane on a porous mixed cellulose ester (MCE) substrate: consecutive spray coating of two liquid crystalline, nematic phases of NaHec with different nanosheet diameter and subsequent cation exchange of the Na^+ interlayer cations with Gua cations.

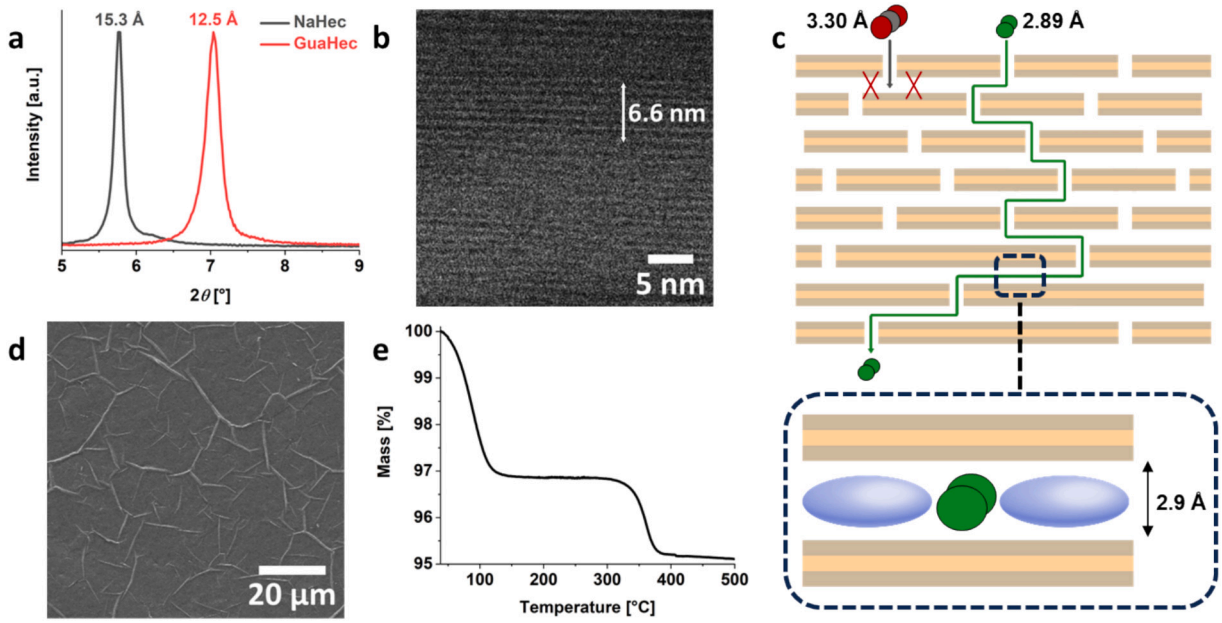

Fig. 2. a) XRD patterns of the NaHec film and the GuaHec membrane. b) Cross-sectional TEM image of the GuaHec membrane. The inserted arrow of ~6.6 nm length corresponds to approximately six basal distances. c) Schematic illustration of the interlayer space-based separation of H_2 in the GuaHec membrane: size-sieving occurs via tortuous path through the interlayer space with a tailored, uniform interlayer height of 2.9 Å, matching the kinetic diameter of H_2, enabling selective H_2 diffusion, while larger gas species, for instance CO_2, are excluded. d) SEM image of the surface of the GuaHec membrane. e) TGA of bulk GuaHec.

methods for the preparation of membranes for selective gas separation by size-sieving in a membrane manufactured by layered building blocks pillared with carbonate anions. For instance, vacuum-suction of a colloidal solution yielded MgAl-CO_3 hydrotalcite, monolithic membranes. The separation performance of these membranes was, however, found to be affected by pinholes and mesoporous intercrystallite voids. These defects were mitigated by post-synthetic coating with a silicone solution, which improved the separation performance (Kim et al., 2009). Membranes were also produced by in-situ growth of layered double hydroxide (LDH) platelets. Compact NiAl-CO_3 LDH (Liu et al., 2014a) or ZnAl-NO_3 LDH (Liu et al., 2014b) membranes fabricated this way were tested for the separation of H_2 and CH_4. In these LDH membranes, platelets are randomly oriented and tend to grow preferentially with their *ab*-direction perpendicular to the substrate. In contrast, silicate monolayers applied in this study are perfectly textured and represent ordered, monodomain 1D crystalline Bragg stacks with a stacking direction perpendicular to the membrane.

Considering a thickness of the silicate nanosheets of 9.6 Å (Stöter et al., 2013), the interlayer height of 5.7 Å in the NaHec film (*d*-value: 15.3 Å, Fig. 2a) is much larger than the kinetic diameter of H_2. Moreover, the hygroscopy of the interlayer cation would render the membrane performance highly sensitive to low levels of moisture producing densely packed water layers in the interlayer space. Therefore, the NaHec film was infiltrated with 1 M solution of Gua chloride to exchange $[Na(H_2O)_6]^+$ with Gua cations (Fig. 1). Energy dispersive X-ray (EDX) spectroscopy confirms a complete exchange of the interlayer

cation as no sodium was detected anymore (**Fig. S4**). According to the chemical composition of pristine NaHec ($[Na_{0.5}]^{inter}[Mg_{2.5}Li_{0.5}]^{oct}[Si_4]^{tet}O_{10}F_2$), this results in a composition of the fabricated GuaHec membrane of $[Gua_{0.5}]^{inter}[Mg_{2.5}Li_{0.5}]^{oct}[Si_4]^{tet}O_{10}F_2$ with a Gua cation content of ~7.4 wt%. As cation exchange is undertaken at high ionic strength, swelling of the prefabricated NaHec film is limited to crystalline swelling and the film does not disintegrate again by 1D dissolution (Rosenfeldt et al., 2016). As Gua is arranged flat lying between the silicate layers and as guanidium is less hydrophilic, upon this cation exchange, the interlayer height of the membrane collapsed to 2.9 Å (*d*-value: 12.5 Å, Fig. 2a). In the interlayer, Gua is not close packed but slit-type micropores between individual pillar molecules exist. The monodomain Bragg stack nature of the GuaHec membrane was confirmed by a cross-sectional transmission electron microscopy (TEM) image (Fig. 2b) and X-ray diffraction, evidenced by a highly rational 00*l*-series with a coefficient of variation <0.75% that indicates a uniform interlayer height. Furthermore, a basal distance of ~11 Å can be estimated from the TEM image, which, within the measurement accuracy (sample may be tilted), agrees to the *d*-value of 12.5 Å for the GuaHec membrane determined by XRD analysis.

This renders the interlayer height selective for H_2 diffusion via tortuous path (Fig. 2c) as the interlayer height (2.9 Å) matches the kinetic diameter of H_2 (2.89 Å (Mehio et al., 2014)). Moreover, the Gua cation mitigates moisture sensitivity of the GuaHec membrane for which swelling does not set in for rH below 90% (Schuchardt et al., 2023). Consequently, the interlayer height is constant up to this rH.

As evidenced by scanning electron microscopy (SEM), the surface of the GuaHec membrane is smooth with a roughness in the range of the nanosheet diameter (Fig. 2d). The borders of overlapping individual nanosheets are clearly visible and no macroscopic defects or pinholes were observed.

The thermal stability of the membrane is only limited by the substrate, for which a mass loss is observed commencing at about 170 °C (**Fig. S5**). The molecular sieve material itself (bulk GuaHec) is stable up to at least 300 °C when decomposition of Gua sets in (Fig. 2e). The fluorosilicate scaffold is stable even up to 800 °C (Ament et al., 2020; Rieß et al., 2020). The mass loss at temperatures <150 °C can be attributed to water molecules adsorbed in the micropores between Gua pillars. Assuming the same molecular volume as for bulk water, a micropore volume of about 0.03 $cm^3\ g^{-1}$ is estimated based on the mass loss associated with water desorption from micropores. This is in good agreement with the micropore volume calculated based on the occupied volume per Gua cation and the charge density of the fluorohectorite (~ 0.03 $cm^3\ g^{-1}$; see Supporting Information for detailed information). The rather low micropore volume limits the solubility of the permeant in the membrane, which certainly is one of the factors limiting the permeance.

3.2. Adsorption and evaluation of the separation performance of the membrane

As expected, the interlayer height of GuaHec is not tall enough to allow larger gas molecules to enter the micropores in the interlayer space. Ar (kinetic diameter of 3.40 Å (Alavi and McDonald, 1990)) physisorption isotherm of bulk GuaHec powder recorded at 87 K showed no porosity over the entire pressure range (**Fig. S6**).

To evaluate the separation performance of the GuaHec membrane, a Wicke-Kallenbach cell was used. The feed gas consisted of 80% H_2 and 20% CO_2, mimicking a typical feedstock found for steam reforming of CH_4 (Ockwig and Nenoff, 2007). The non-coated MCE substrate shows permeances for H_2 and CO_2 > 5000 gas permeation units (GPU; 1 GPU = 10^{-6} $cm^3\ cm^{-2}\ s^{-1}\ cmHg^{-1}$) with a H_2/CO_2 selectivity <1, exactly matching the results for an empty sample cell indicating no influence of the substrate on the separation of these two gases (**Fig. S7**). With the GuaHec membrane the H_2 permeance was substantially reduced to 3 GPU at ambient conditions (23.4 °C and 1 bar, Fig. 3). This had to be expected according to tortuous path theory. Compared to other

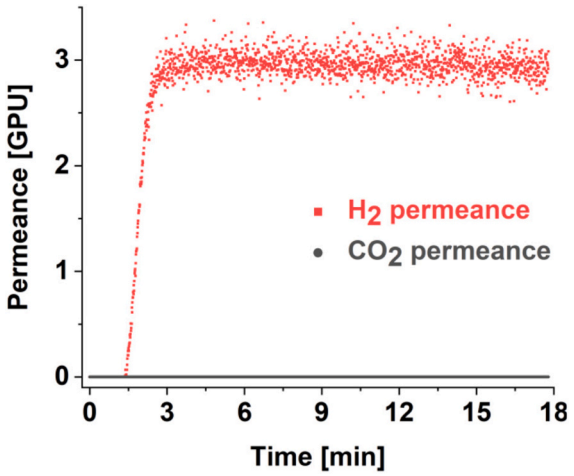

Fig. 3. Evaluation of the separation performance of the GuaHec membrane: H_2 and CO_2 permeance vs. time.

heterostructured membranes, this value is rather low. For instance, for a Co-ZIF-9 tubular membrane a H_2 permeance of ~480 GPU was reported for a binary 1:1 H_2/CO_2 mixture at similar conditions (25 °C, 1 bar) with a H_2/CO_2 separation factor of ~19 (Nian et al., 2018). The values for the H_2 permeance <3 GPU obtained within the first three minutes of the measurement can be attributed to the filling of the dead volume of the measurement setup. Subsequently, a plateau with a constant value of 3 GPU is reached for the H_2 permeance. While the permeance is a downside of our membrane material, an outstanding near-perfect H_2/CO_2 separation factor was observed since CO_2 was not detectable in the permeate (detection limit minimum <20 ppm). Size-sieving via a well-defined tailored interlayer height of 2.9 Å works efficiently as larger CO_2 is completely excluded from entering the interlayer space.

4. Conclusion

Quite a few successful attempts to achieve efficient molecular sieving for H_2/CO_2 separation have been reported in literature. Tailoring the interlayer height in an easy and reproducible way is key for selectivity. Of equal importance is facial fabrication of defect-free monodomain membranes. Ionic nanosheets of uniform thickness produced by 1D dissolution bear great potential to address both these challenges. As the number of layered materials that can be delaminated by 1D dissolution is steadily increasing, a modular toolbox becomes available to fabricate permselective membranes via the route introduced in this manuscript for layered silicate nanosheets: i) obtain nematic suspensions by 1D dissolution, ii) fabricate membranes by self-assembly into monodomain Bragg stacks, iii) tailor the interlayer height to obtain selectivity by appropriate molecular pillars. With a plethora of pillars available, the last step renders the approach generally applicable to separate gases of even slightly different kinetic radius. While the selectivity observed with this first study is superb, permeance clearly is unacceptably low.

However, this downside may be overcome in future work, as there is large scope for potential improvements, and optimization is possible via several parameters. For example, the aspect ratio of the nanosheets in the membrane body could be further reduced, thereby shortening the tortuous path for H_2 molecules, which would result in an increased permeance. In addition, it must be checked whether the primer coat with the large platelets, significantly reducing the permeance of the membrane, is actually necessary or whether at least its thickness may be reduced applying a less corrugated substrate. Another, albeit much more complex method of membrane preparation would be the use of a gradient in platelet size in order to enhance the permeance. Reducing the membrane thickness, e.g. by reducing the number of spray cycles or by using a suspension with a lower concentration of nanosheets, should

also have positive effect on the permeance. To increase the micropore volume two measures may be taken: 1. The equivalent area of the pillar might furthermore be reduced by ~10% applying formamidinium instead of Gua. 2. The charge density of the silicate layers might be lowered and hence the Gua loading will be reduced. However, all of these suggestions for an improvement of membrane performance in terms of permeance are, of course, only constructive if the quality of the membrane is ensured and the superb selectivity thus is not affected.

5. Associated content

Supporting information (pdf): SLS analyses of highly diluted NaHec suspensions of large platelets (as-synthesized) and small platelets (shredded). SEM image and corresponding EDX analysis of the GuaHec membrane. TGA of the non-coated MCE substrate. Ar physisorption isotherm of bulk GuaHec recorded at 87.35 K. H_2 and CO_2 permeance vs. time with the empty cell and with the pure MCE substrate, respectively. XRD pattern of bulk GuaHec. SEM image and corresponding EDX analysis of bulk GuaHec. Equations for determination of permeance and separation factor from measurements with Wicke-Kallenbach cell.

CRediT authorship contribution statement

Lukas Federer: Visualization, Validation, Methodology, Investigation, Formal analysis, Data curation, Writing – review & editing, Writing – original draft. **Ingmar Pietsch:** Data curation, Writing – review & editing. **Felix Uhlig:** Data curation, Writing – review & editing. **Max Stevenson:** Data curation, Writing – review & editing. **Daniel Friedrich:** Visualization, Writing – review & editing. **Josef Breu:** Validation, Supervision, Resources, Project administration, Methodology, Funding acquisition, Data curation, Conceptualization, Writing – review & editing.

Declaration of competing interest

The authors declare no competing interests.

Acknowledgments

The authors thank Marco Schwarzmann for measuring the cross-sectional TEM and the SEM images, performing the EDX analyses and carrying out the TGA experiments. The authors appreciate the support of the Keylab for Optical and Electron Microscopy of the Bavarian Polymer Institute. The authors thank Florian Puchtler and the Keylab for Polymer Additives and Fillers of the Bavarian Polymer Institute for synthesis of the NaHec.

Appendix A. Supplementary data

Supplementary data to this article can be found online at https://doi.org/10.1016/j.clay.2026.108191.

Data availability

Data will be made available on request.

References

Abd-Elrahim, A., Chun, D.-M., 2022. One-step mechanical exfoliation and deposition of layered materials (graphite, MoS_2, and BN) by vacuum-kinetic spray process. Vacuum 196, 110732. https://doi.org/10.1016/j.vacuum.2021.110732.

Adhikari, S., Fernando, S., 2006. Hydrogen membrane separation techniques. Ind. Eng. Chem. Res. 45 (3), 875–881. https://doi.org/10.1021/ie050644l.

Agrawal, K.V., Zhang, X., Elyassi, B., Brewer, D.D., Gettel, M., Kumar, S., Lee, J.A., Maheshwari, S., Mittal, A., Sung, C.-Y., 2011. Dispersible exfoliated zeolite nanosheets and their application as a selective membrane. Science 334 (6052), 72–75. https://doi.org/10.1126/science.1208891.

Alavi, A., McDonald, I.R., 1990. Molecular-dynamics simulation of argon physisorbed on magnesium oxide. Mol. Phys. 69 (4), 703–713. https://doi.org/10.1080/00268979000100521.

Al-Mufachi, N.A., Rees, N.V., Steinberger-Wilkens, R., 2015. Hydrogen selective membranes: a review of palladium-based dense metal membranes. Renew. Sust. Energ. Rev. 47, 540–551. https://doi.org/10.1016/j.rser.2015.03.026.

Ament, K., Wagner, D.R., Meij, F.E., Wagner, F.E., Breu, J., 2020. High temperature stable maghemite nanoparticles sandwiched between hectorite nanosheets. Z. Anorg. Allg. Chem. 646 (14), 1110–1115. https://doi.org/10.1002/zaac.202000077.

Bredesen, R., Jordal, K., Bolland, O., 2004. High-temperature membranes in power generation with CO_2 capture. Chem. Eng. Process. Process Intensif. 43 (9), 1129–1158. https://doi.org/10.1016/j.cep.2003.11.011.

Breu, J., Seidl, W., Stoll, A.J., Lange, K.G., Probst, T.U., 2001. Charge Homogeneity in Synthetic Fluorohectorite. Chem. Mater. 13 (11), 4213–4220. https://doi.org/10.1021/cm011014m.

Chuah, C.Y., Lee, J., Bae, T.-H., 2020. Graphene-based membranes for H_2 separation: recent progress and future perspective. Membranes 10 (11), 336. https://doi.org/10.3390/membranes10110336.

Dakhchoune, M., Villalobos, L.F., Semino, R., Liu, L., Rezaei, M., Schouwink, P., Avalos, C.E., Baade, P., Wood, V., Han, Y., 2021. Gas-sieving zeolitic membranes fabricated by condensation of precursor nanosheets. Nat. Mater. 20 (3), 362–369. https://doi.org/10.1038/s41563-020-00822-2.

DeRocher, J.P., Gettelfinger, B.T., Wang, J., Nuxoll, E.E., Cussler, E.L., 2005. Barrier membranes with different sizes of aligned flakes. J. Membr. Sci. 254 (1–2), 21–30. https://doi.org/10.1016/j.memsci.2004.12.025.

Dudko, V., Khoruzhenko, O., Weiß, S., Daab, M., Loch, P., Schwieger, W., Breu, J., 2023. Repulsive osmotic delamination: 1D dissolution of 2D materials. Adv. Mater. Technol. 8 (3), 2200553. https://doi.org/10.1002/admt.202200553.

Ellis, G.S., Gelman, S.E., 2024. Model predictions of global geologic hydrogen resources. Sci. Adv. 10 (50), eado0955. https://doi.org/10.1126/sciadv.ado0955.

Habel, C., Tsurko, E.S., Timmins, R.L., Hutschreuther, J., Kunz, R., Schuchardt, D.D., Rosenfeldt, S., Altstädt, V., Breu, J., 2020. Lightweight ultra-high-barrier liners for helium and hydrogen. ACS Nano 14 (6), 7018–7024. https://doi.org/10.1021/acsnano.0c01633.

Hassan, N.S., Jalil, A.A., Rajendran, S., Khusnun, N.F., Bahari, M.B., Johari, A., Kamaruddin, M.J., Ismail, M., 2024. Recent review and evaluation of green hydrogen production via water electrolysis for a sustainable and clean energy society. Int. J. Hydrog. Energy 52, 420–441. https://doi.org/10.1016/j.ijhydene.2023.09.068.

Heinke, L., Tu, M., Wannapaiboon, S., Fischer, R.A., Wöll, C., 2015. Surface-mounted metal-organic frameworks for applications in sensing and separation. Microporous Mesoporous Mater. 216, 200–215. https://doi.org/10.1016/j.micromeso.2015.03.018.

Holladay, J.D., Hu, J., King, D.L., Wang, Y., 2009. An overview of hydrogen production technologies. Catal. Today 139 (4), 244–260. https://doi.org/10.1016/j.cattod.2008.08.039.

Kim, W.-G., Nair, S., 2013. Membranes from nanoporous 1D and 2D materials: a review of opportunities, developments, and challenges. Chem. Eng. Sci. 104, 908–924. https://doi.org/10.1016/j.ces.2013.09.047.

Kim, T.W., Sahimi, M., Tsotsis, T.T., 2009. The preparation and characterization of hydrotalcite thin films. Ind. Eng. Chem. Res. 48 (12), 5794–5801. https://doi.org/10.1021/ie900371r.

Li, H., Haas-Santo, K., Schygulla, U., Dittmeyer, R., 2015. Inorganic microporous membranes for H_2 and CO_2 separation—review of experimental and modeling progress. Chem. Eng. Sci. 127, 401–417. https://doi.org/10.1016/j.ces.2015.01.022.

Liu, Y., Wang, N., Cao, Z., Caro, J., 2014a. Molecular sieving through interlayer galleries. J. Mater. Chem. A 2 (5), 1235–1238. https://doi.org/10.1039/C3TA13792A.

Liu, Y., Wang, N., Caro, J., 2014b. In situ formation of LDH membranes of different microstructures with molecular sieve gas selectivity. J. Mater. Chem. A 2 (16), 5716–5723. https://doi.org/10.1039/C4TA00108G.

Liu, Y., Pan, J.H., Wang, N., Steinbach, F., Liu, X., Caro, J., 2015. Remarkably enhanced gas separation by partial self-conversion of a laminated membrane to metal–organic frameworks. Angew. Chem. 127 (10), 3071–3075. https://doi.org/10.1002/ange.201411550.

Mehio, N., Dai, S., Jiang, D.-E., 2014. Quantum mechanical basis for kinetic diameters of small gaseous molecules. J. Phys. Chem. A 118 (6), 1150–1154. https://doi.org/10.1021/jp412588f.

Miłek, D., Nowak, P., Latosińska, J., 2022. The development of renewable energy sources in the European Union in the light of the European Green Deal. Energies 15 (15), 5576. https://doi.org/10.3390/en15155576.

Nian, P., Li, Y., Zhang, X., Cao, Y., Liu, H., Zhang, X., 2018. ZnO nanorod-induced heteroepitaxial growth of SOD type Co-based zeolitic imidazolate framework membranes for H_2 separation. ACS Appl. Mater. Interfaces 10 (4), 4151–4160. https://doi.org/10.1021/acsami.7b17568.

Nunnenkamp, M., van den Nieuwenhuijzen, K.J., Ten Elshof, J.E., 2022. Multilayer films of exfoliated 2D oxide nanosheets by electrospray deposition. Sci. Rep. 12 (1), 8673. https://doi.org/10.1038/s41598-022-12768-3.

Ockwig, N.W., Nenoff, T.M., 2007. Membranes for hydrogen separation. Chem. Rev. 107 (10), 4078–4110. https://doi.org/10.1021/cr0501792.

Peng, Y., Li, Y., Ban, Y., Jin, H., Jiao, W., Liu, X., Yang, W., 2014. Metal-organic framework nanosheets as building blocks for molecular sieving membranes. Science 346 (6215), 1356–1359. https://doi.org/10.1126/science.1254227.

Rieß, M., Siegel, R., Senker, J., Breu, J., 2020. Diammonium-Pillared MOPS with Dynamic CO_2 Selectivity. Cell Rep. Phys. Sci. 1 (10), 100210. https://doi.org/10.1016/j.xcrp.2020.100210.

Ritter, J.A., Ebner, A.D., 2007. State-of-the-art adsorption and membrane separation processes for hydrogen production in the chemical and petrochemical industries. Sep. Sci. Technol. 42 (6), 1123–1193. https://doi.org/10.1080/01496390701242194.

Rosenfeldt, S., Stöter, M., Schlenk, M., Martin, T., Albuquerque, R.Q., Förster, S., Breu, J., 2016. In-depth insights into the key steps of delamination of charged 2D nanomaterials. Langmuir 32 (41), 10582–10588. https://doi.org/10.1021/acs.langmuir.6b02206.

Sazali, N., Mohamed, M.A., Salleh, W.N.W., 2020. Membranes for hydrogen separation: a significant review. Int. J. Adv. Manuf. Technol. 107 (3), 1859–1881. https://doi.org/10.1007/s00170-020-05141-z.

Schuchardt, D., Röhrl, M., Federer, L., Rosenfeldt, S., Kalo, H., Breu, J., 2023. Spraying transparent nanoglass coatings for food packaging. ACS Appl. Nano Mater. 6 (18), 17000–17008. https://doi.org/10.1021/acsanm.3c03144.

Shi, M., Li, X., Jiang, Y., Li, S., Li, B., Zhang, X., Zhang, S., Nan, C.W., 2023. 2D nanosheet spray coating for scalable processing of high-energy-density dielectric polymer films. Adv. Electron. Mater. 9 (7), 2300187. https://doi.org/10.1002/aelm.202300187.

Sircar, S., Golden, T.C., 2000. Purification of hydrogen by pressure swing adsorption. Sep. Sci. Technol. 35 (5), 667–687. https://doi.org/10.1081/SS-100100183.

Spillman, R.W., 1989. Economics of gas separation membranes. Chem. Eng. Prog. 85 (1), 41–62. https://doi.org/10.5555/19891932222.

Stöter, M., Kunz, D.A., Schmidt, M., Hirsemann, D., Kalo, H., Putz, B., Senker, J.r., Breu, J., 2013. Nanoplatelets of sodium hectorite showing aspect ratios of≈ 20 000 and superior purity. Langmuir 29 (4), 1280–1285. https://doi.org/10.1021/la304453h.

Sudo, H., Nishina, Y., Imai, H., Oaki, Y., 2025. 2D nanoarchitectonics for exfoliated nanosheets: tailoring surface roughness of thin-film coatings. Nanoscale 17 (47), 27362–27369. https://doi.org/10.1039/D5NR03769G.

Sun, S., Li, S., Wang, S., Chen, Y., 2024. Design and development of highly selective and permeable membranes for H_2/CO_2 separation—a review. Chem. Eng. J., 152972 https://doi.org/10.1016/j.cej.2024.152972.

Tsurko, E.S., Feicht, P., Nehm, F., Ament, K., Rosenfeldt, S., Pietsch, I., Roschmann, K., Kalo, H., Breu, J., 2017. Large scale self-assembly of smectic nanocomposite films by doctor blading versus spray coating: impact of crystal quality on barrier properties. Macromolecules 50 (11), 4344–4350. https://doi.org/10.1021/acs.macromol.7b00701.

Wang, Y., Ma, X., Ghanem, B.S., Alghunaimi, F., Pinnau, I., Han, Y., 2018. Polymers of intrinsic microporosity for energy-intensive membrane-based gas separations. Mater. Today Nano 3, 69–95. https://doi.org/10.1016/j.mtnano.2018.11.003.

Wappler, M., Unguder, D., Lu, X., Ohlmeyer, H., Teschke, H., Lueke, W., 2022. Building the green hydrogen market–current state and outlook on green hydrogen demand and electrolyzer manufacturing. Int. J. Hydrog. Energy 47 (79), 33551–33570. https://doi.org/10.1016/j.ijhydene.2022.07.253.

Yue, M., Lambert, H., Pahon, E., Roche, R., Jemei, S., Hissel, D., 2021. Hydrogen energy systems: a critical review of technologies, applications, trends and challenges. Renew. Sust. Energ. Rev. 146, 111180. https://doi.org/10.1016/j.rser.2021.111180.

Zhou, Y., LaChance, A.M., Smith, A.T., Cheng, H., Liu, Q., Sun, L., 2019. Strategic design of clay-based multifunctional materials: from natural minerals to nanostructured membranes. Adv. Funct. Mater. 29 (16), 1807611. https://doi.org/10.1002/adfm.201807611.